Compact AFSIW Antenna with Integrated Digitally Controlled Impedance Tuner for Smart Surfaces

Joryan Sennesael, *Student Member, IEEE,* Kamil Yavuz Kapusuz, *Member, IEEE,* Sam Lemey, *Member, IEEE,* Patrick Van Torre, *Member, IEEE,* and Hendrik Rogier, *Senior Member, IEEE*

***Abstract*—For unobtrusive smart-surface integration, an air-filled substrate-integrated waveguide (AFSIW) antenna for the [5.15-5.85] GHz band is co-designed with a tunable matching network and a cavity-integrated biasing circuit. It features a reconfigurable matching network to mitigate impedance mismatch due to objects in its reactive near field. A digitally controlled biasing circuit with switched-mode power supply is seamlessly integrated inside the air-filled antenna cavity to accurately control the matching network through a serial interface. The proposed impedance-tunable antenna covers an impedance bandwidth from 4.64 GHz to 6.09 GHz with a peak gain of 4.51 dBi at its center frequency. Measurements show that the cavity-integrated circuitry has negligible influence on the antenna performance, yielding novel integration potential. The impedance-tunable antenna is tested in a smart surface desktop integration scenario where it corrects detuning by objects placed on top, improving the wireless link for IEEE 802.11ac bands.**

***Index Terms*—Air-filled substrate integrated waveguide (AFSIW), cavity-backed slot antenna, Internet of Things (IoT), reconfigurable matching network, smart surfaces.**

I. Introduction

THE Internet of Things (IoT) increases demand for wireless interconnected devices in both domestic and industrial environments [1]. Smart devices, seamlessly and invisibly integrated in everyday objects and surfaces, such as an office desk, offer added connectivity [2], [3], but their performance should not be compromised by deployment conditions or external influences, such as nearby objects or people in the reactive near field of the antennas [4].

For stable high data-rate communication, the surface-integrated antennas must retain good impedance matching, low insertion loss and high isolation, even when external influences, such as objects or people near the antenna, detune their impedance and compromise the total antenna efficiency. Similarly, surface integration may also affect antenna behavior [2], [3]. Impedance mismatch increases the voltage standing wave ratio (VSWR), potentially damaging the amplifier and introducing inter-symbol interference on transmission lines [5]. Furthermore, the performance of radio frequency (RF) amplifiers in terms of power-added efficiency and 1 dB compression point strongly depends on the load-pulling effects of the specific antenna impedance [6]. Hence, reconfigurable antenna systems that adaptively match the antenna impedance to the amplifier are needed for consistent link quality.

In the past, reconfigurable matching networks and filters were exploited to counteract antenna detuning. Using PIN diodes to switch circuit elements [7]–[9] generally leads to diode losses and a limited number of discrete states. Relying on MEMS switches [10] or MEMS varactors [11] yields significantly lower losses and size reduction, but is more expensive and often requires high control voltages that are difficult to achieve in IoT applications. Custom CMOS-switched capacitors and chips offer good tuning performance, albeit at sub-GHz frequencies and at significantly higher production cost [12], [13]. Finally, varactor diodes achieve a good trade-off between tunability and losses, while being comparatively cheap [14], [15]. Currently, such networks are integrated into the antenna to reduce interconnection losses, yielding a cheap, compact solution [8], [13], [16]. However, a seamless integration of an impedance-reconfigurable antenna with its biasing electronics has not been studied before, nor were such devices tested in a real surface-integration scenario.

This paper presents the first air-filled substrate integrated waveguide (AFSIW) antenna co-designed with a tunable matching network and cavity-integrated biasing circuit for smart surfaces. In contrast to [17], where PIN diodes are integrated at the top of the AFSIW, the proposed design incorporates the entire biasing circuit of a tunable matching network, including a DC-DC converter to step up the voltage, inside the antenna air cavity. Furthermore, the reconfigurable matching network itself is implemented on the antenna's back side, where it is shielded from the antenna's EM field. To the author's best knowledge, this is the first impedance-tunable AFSIW antenna that implements a complete varactor biasing network and switched-mode power supply (SMPS) inside the air-filled cavity while ensuring that the integrated electronics have negligible influence on RF performance. The AFSIW technology yields a wide impedance bandwidth, stable antenna gain and high antenna efficiency. The proposed system provides digitally controlled adaptive impedance matching over a large region of the Smith chart to correct antenna detuning. Furthermore, the direct and compact integration of antenna and matching network with its control circuit reduces losses and parasitics, yields higher transmission efficiency and serves as protective casing for the integrated circuitry.

II. Description of the System

A tunable AFSIW antenna system for integration in smart surfaces is designed for operation in the [5.15-5.85] GHz IEEE 802.11ac WIFI 5 bands with a return loss larger than 10 dB, even when affected by objects in its reactive near field. Furthermore, the complete system must achieve a sufficiently high antenna efficiency ($> 50\%$) after integration in a smart surface. Hence, the matching network's insertion loss must

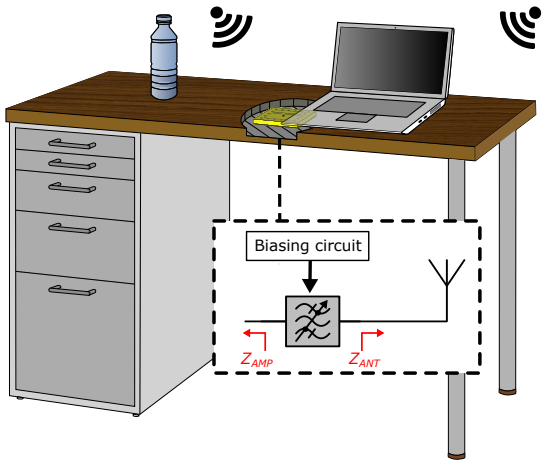

Fig. 1. Representative application with the impedance-tunable antenna integrated in a smart surface to counteract influences of objects placed on the desktop.

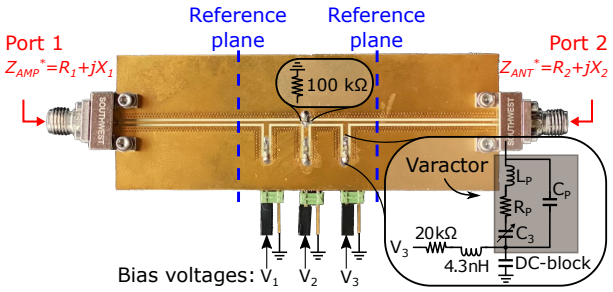

Fig. 2. Fabricated stand-alone prototype of the proposed matching network with schematic representation of discrete components and varactor parasitics (L_p = 0.2 nH, R_p = 1 Ω, C_p = 0.1 pF), using a 3 pF DC-blocking capacitor. The TRL-calibrated reference planes are indicated by blue lines.

remain smaller than 3 dB. Fig. 1 presents a potential use case, with the system invisibly integrated in a desk surface. Objects or people in its direct vicinity detune its impedance, deteriorating the wireless link performance. The integrated reconfigurable matching network corrects this mismatch and optimizes power transfer.

A. Reconfigurable matching network

A tunable matching network is designed based on a Chebyshev band-pass topology [18] with 50% fractional bandwidth at 5.5 GHz center frequency. To reduce spurious radiation, the circuit is implemented in grounded co-planar waveguide (GCPW) technology on a 254-μm-thick I-Tera substrate (ϵ_r = 3.43 and $\tan\delta$ = 0.014 at 5.5 GHz), relying on shorted $\lambda/4$ transmission-line stubs with tunable varactors at their ends, each controlled by a well-decoupled bias voltage, as shown in Fig. 2. Given the non-idealities of the varactor diodes and substrate, a 3rd-order topology with three tunable stubs was adopted as a trade-off between tuning range and losses. For a 5th or higher order filter, the losses in the varactor's junction capacitance and the physical size of the board would become a limiting factor, while a filter order lower than three would significantly reduce tuning range.

MPV1965 varactors by Microsemi were selected with a capacitance tuning range from 0.55 pF (15 V reverse bias) to 4.8 pF (0 V reverse bias) in the frequency band of interest. To ensure an unobstructed RF path through the varactor stubs, a 3 pF high-Q-factor capacitor is applied at its self-resonance frequency as DC-block (Fig. 2) between the DC bias voltage and ground, thereby reducing the magnitude of the RF impedance below 2.13 Ω over the entire operating band. The complete voltage and frequency dependent behavior of the varactor diodes and decoupling capacitors, including parasitics, is characterized by a custom thru-reflect-line (TRL) calibrated board.

Starting from the prototype lumped-element value definitions (g_0=g_4=1, g_1=g_3=1.0316, g_2=1.1474) of a 3rd-order low-pass Chebyshev filter with 0.1 dB ripple, a band-pass filter is conceived by performing a frequency transformation, as described in [18]. Subsequently, the impedances of the $\lambda/4$ transmission lines are dimensioned and varactors are added at the end of the three shorted stubs. Based on the varactor's equivalent circuit, the stubs are adapted such that applying no voltage to the varactors (nominal bias point) yields a 50 Ω impedance at both sides of the reconfigurable matching network. Increasing the reverse bias voltages on the varactors changes the impedance of the corresponding stubs, thereby tuning the impedance of the ports. Hence, by applying the correct biasing voltages, the filter acts as a broadband matching network. Furthermore, the symmetric design enables the same impedance transformation at both the amplifier and antenna side.

B. Biasing circuit

To exploit the full capacitance range of the MPV1965 varactors, their reverse voltage must be reconfigurable between 0 V and 15 V. These voltages are provided by a robust biasing circuit that is later implemented inside the antenna's (Fig. 3) AFSIW cavity (Fig. 4). This circuit is digitally controlled. It only requires a four-wire digital interface, consisting of a 5 V DC power supply and ground, together with clock and data lines that support serial communication over the I2C protocol.

First, the three separate varactor-diode bias voltages are generated by an 8-channel 12-bit DAC7876 (Digital-to-Analog Converter) by Texas Instruments, in a compact QFN-24 package. This DAC features a 2.5 V internal reference with a 5 mV accuracy, allowing precise tuning between 0 to 5 V. Next, this voltage is scaled up by a factor of four to cover the full tuning range of the MPV1965 varactor diodes, while providing sufficient headroom. This is achieved by a non-inverting rail-to-rail operational amplifier (opamp), in a compact 14-pin X2QFN package. The amplifier output biases the varactors. The RF signal flowing through the varactors is isolated from the opamp's output by a 4.3 nH inductor in series with a 20 kΩ resistor and instead is grounded by a 3 pF DC-block capacitor, as shown in Fig. 2. Finally, to achieve bias voltages above the 5 V input supply, a small-scale boost converter is added using the LT8330 IC by Analog Devices in its compact 8-pad DFN package. The switching frequency of 2 MHz allows using a physically small inductor of 1 μH in a 0402 package. The remaining switching noise is significantly suppressed by an LM7824 voltage regulator in a SOT-89 package, yielding a

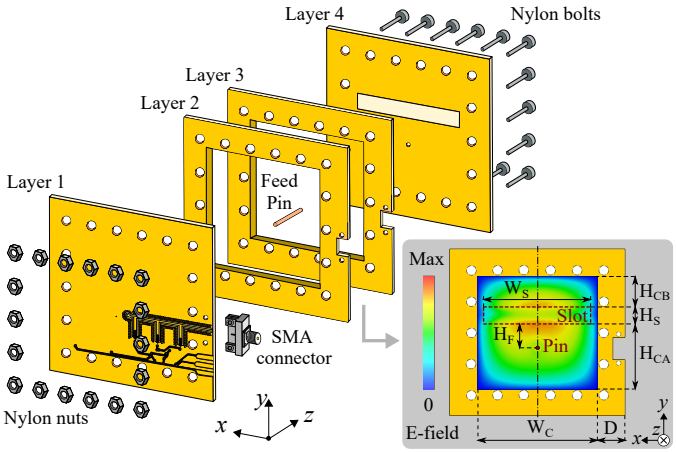

Fig. 3. Detailed fabrication procedure of the proposed AFSIW antenna with integrated reconfigurable matching network and biasing electronics (exploded view) with sub-figure of the simulated electric field inside the cavity illustrated by a logarithmic color scale. Antenna dimensions: $W_S = 38$ mm, $W_C = 42$ mm, $D = 10$ mm, $H_{CA} = 24$ mm, $H_S = 5.5$ mm, $H_{CB} = 11$ mm, $H_F = 12.15$ mm.

precise 24 V to feed the opamps. The average power consumption of this circuit remains below 10 mW for all bias settings.

C. Integration in AFSIW antenna

A coupled half-mode cavity-backed slot antenna is designed in AFSIW technology as a robust planar integration platform for deployment in smart surfaces, since it provides a large bandwidth [17], high front-to-back-ratio (FTBR) [3], strong isolation from its environment [3] and an air region inside the antenna cavity that can be exploited to integrate electronic components [17]. The antenna is fabricated using a stack-up of four dual-layer mass-producible PCBs (Printed Circuit Boards), as shown in Fig. 3. The two outer layers (Layer 1 and 4) are manufactured in a 0.254-mm-thick I-Tera high-frequency laminate. The two inner layers (Layer 2 and 3) are realised in 1.55-mm-thick low-cost FR-4 material, relying on edge-plating technology to create the AFSIW cavity's conductive walls. All layers are assembled by nylon alignment bolts that fit through plated via holes. The antenna is fed by a 1.3 mm copper pin running from Layer 1 to Layer 4. A slot in the ground plane of Layer 4 serves as the antenna's aperture, thereby enabling radiation in the $+z$-direction.

Layer 1 of the antenna incorporates both the reconfigurable matching network and the biasing electronics, enabling significant cost savings and a compact design. The reconfigurable matching network is implemented on the backside of the AFSIW antenna, where it is largely shielded from the antenna's electromagnetic field, owing to the underlying ground plane at the other side of the PCB. A Southwest SMA (SubMiniature version A) connector is used to edge-feed the matching network, which in turn injects the RF signal into the antenna cavity through the before-mentioned copper pin.

The biasing circuit for the reconfigurable matching network is implemented on the front side of Layer 1. Since these components are integrated inside the AFSIW cavity, they will be subject to its strong EM-field. Hence, the circuit has to be well designed such that its operation remains unaffected after integration, while the impact on the antenna performance

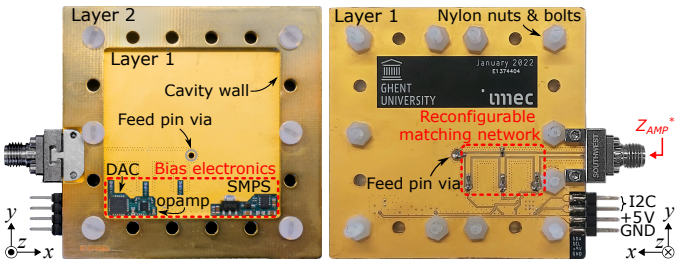

Fig. 4. Detailed view of integrated biasing electronics inside the AFSIW cavity (left) and reconfigurable matching network on the back side of the fabricated antenna prototype (right).

remains minimal. A full-wave simulation of the electric field inside the cavity, shown as a sub-figure of Fig. 3 together with all relevant antenna dimensions, suggests that the best location for electronic components in the cavity is near the corners and the edges, since there the field strength is at its minimum. Taking into account these design considerations, the biasing electronics were compactly implemented near the corners of the lower half-mode cavity of the AFSIW, as shown in Fig. 4. By concentrating all the DAC- and opamp-related circuitry on the left side of the cavity and the entire SMPS on the right, the circuit can be effectively split up, requiring only two DC traces on the backside of the antenna. As a result, the ground plane inside the cavity remains almost unaffected by the integration of these components. A minimal solder mask region around the components ensures a straightforward reflow-soldering process for large-scale fabrication without introducing significant substrate losses.

III. Measurements

Prototypes of the proposed fully integrated system, together with a stand-alone version of both the tunable matching network and AFSIW antenna were fabricated and characterized. All S-parameter measurements were performed with a Keysight PNA E8364B vector network analyser (VNA). The radiation patterns were measured in an anechoic chamber, relying on an NSI-700S-30 positioning system paired with a Keysight PNA-X N5242B VNA. During these measurements, a 5 V battery pack powered the impedance-tunable antenna's biasing electronics while the tuning system was programmed using an STM32 development board.

Making use of a custom TRL calibration kit, the stand-alone matching network (Fig. 2) was de-embedded and fully characterized over the complete tuning range of the board. Fig. 5 illustrates all obtainable output impedances on a Smith chart, when terminating port 1 by 50 Ω. Hence, the colored areas indicate the impedances that the tuner can transform to 50 Ω. As a benchmark, the tuner can transform 100%, 85% and 63% of the impedance values within the VSWR ≤ 3 circle to 50 Ω at 5.15 GHz, 5.50 GHz and 5.85 GHz, respectively. Yet, such a comparison could be made for any given VSWR circle. For the nominal bias point (0 V applied to all varactors), the network achieves a fractional impedance bandwidth ($|S_{11}| <$ -10 dB) of 46%, which closely resembles the designed 50%. Furthermore, a low insertion loss of 1.69 dB (via a simulated model estimated to be composed of less than 1% radiation

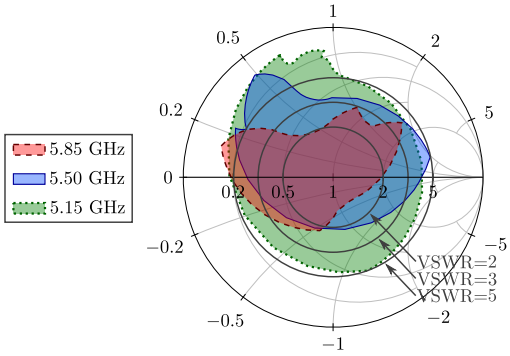

Fig. 5. Measured output impedance range of the de-embedded prototype of the stand-alone tunable matching network at port 2 (w.r.t. 50 Ω, when terminating port 1 by 50 Ω). The VSWR circles serve as a benchmark.

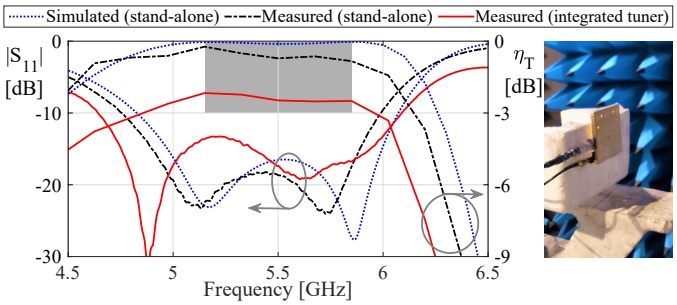

Fig. 6. Reflection coefficient $|S_{11}|$ and total antenna efficiency η_T of the stand-alone and impedance-tunable antenna at the nominal bias point (0 V applied to all varactors).

loss, 32% dielectric loss, 11% conductor loss and 56% losses in varactors/capacitors) is achieved at 5.5 GHz, while staying below 1.83 dB over the entire band of interest.

Fig. 6 shows the magnitude of the reflection coefficient $|S_{11}|$ and total antenna efficiency η_T of the stand-alone antenna compared to the proposed antenna with integrated impedance tuner and biasing electronics. The results are in good agreement with the expectations, with the impedance-reconfigurable antenna achieving a slightly wider impedance bandwidth from 4.64 GHz to 6.09 GHz due to the influence of the matching network. The measured total antenna efficiency of the impedance-tunable antenna equals 57% (-2.47 dB) at 5.5 GHz versus 85% (-0.72 dB) for the stand-alone antenna. This difference of 1.75 dB can be mainly attributed to the insertion loss of the de-embedded matching network, measured to be 1.69 dB. Furthermore, simulations show that the GCPW-to-coaxial transition and the SMA connector account for a combined loss below 0.08 dB. This indicates that the integration of the biasing electronics in the air-filled cavity has almost no influence on the efficiency of the antenna.

Fig. 7 shows the radiation patterns of the stand-alone and impedance-tunable antenna prototypes at the center frequency of 5.5 GHz. The impedance-tunable antenna achieves a maximum gain of 4.51 dBi, compared to 6.58 dBi for the stand-alone antenna, due to the earlier discussed losses and a slightly increased half-power beamwidth (HPBW) of 119° in the YZ-plane (ϕ = 90°), versus 107°, with both achieving a 69° HPBW in the XZ-plane (ϕ = 0°). Furthermore, for both antenna prototypes the FTBR exceeds 30 dB while the

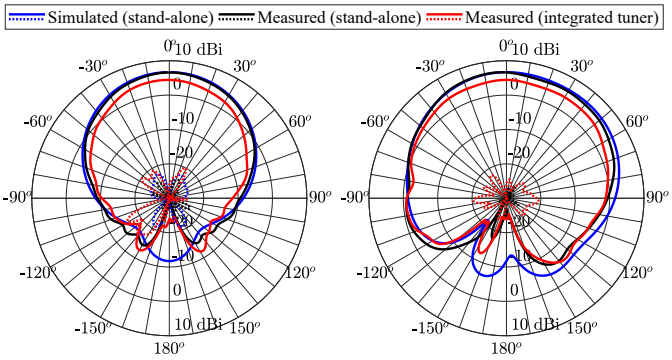

Fig. 7. Co-polarisation (——) and cross-polarisation (·····) radiation patterns of stand-alone antenna, and antenna with integrated impedance tuner and biasing electronics, in the XZ-plane (ϕ = 0°, left column) and YZ-plane (ϕ = 90°, right column), at 5.50 GHz.

cross-polarization level remains below -20 dB over the entire HPWB. Within the frequency band of interest, the gain of the impedance-tunable antenna is flat, with a ripple of 0.305 dB. Hence, judiciously integrating circuitry in the AFSIW cavity has negligible effect on the performance, thereby proving its novel integration potential.

To illustrate the proposed system's operation in a real-world application, a link experiment was conducted to compare both the stand-alone antenna and impedance-tunable antenna when integrated in a Medium Dense Fiber (MDF) board and covered by an High Pressure Laminate (HPL), simulating a desk acting as smart surface, previously proposed in Fig. 1. The test setup, shown in Fig. 8(a) to (d), has an identical stand-alone antenna mounted 25 cm above the desktop surface to perform a two-port link measurement at 0 dBm transmit power. The desk-integrated antennas were detuned by placing a laptop and flash drive on top of the desk surface, thereby deteriorating the matching and link performance. Fig. 8 shows the reflection coefficient and power received by the stand-alone antenna versus the tuner antenna, optimized for operation in IEEE 802.11ac channels 50, 114 and 155, by tuning the biasing voltages such that the received power is maximized while keeping the antenna matched. Note that more advanced optimization algorithms have already been extensively researched [19] and could be paired with an in-line impedance sensor [20] to achieve full autonomy. During all conducted tests, the proposed antenna system achieved good matching whereas the stand-alone antenna suffered from significant reflections. Furthermore, the link budget also increased in most scenarios, despite the losses introduced by the matching network.

Table I compares the performance of the proposed reconfigurable matching network to the current state-of-the-art. It is clear that our topology features a large impedance bandwidth and low losses, especially compared to other varactor-based solutions, while facilitating a compact integration of the circuit within the antenna footprint. Moreover, owing to a dedicated design and integration strategy, the proposed system maintains stable antenna performance, even after directly implementing biasing electronics inside the antenna cavity, in contrast to other state-of-the-art designs.

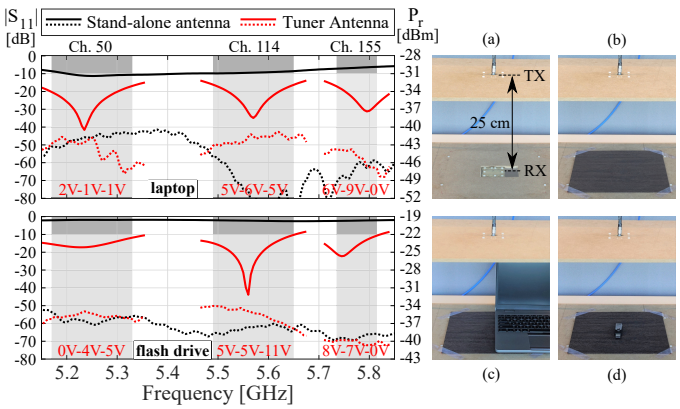

Fig. 8. Magnitude of reflection coefficient $|S_{11}|$ (——) and received power level P_r (·····) by antenna disturbed by a laptop and flash-drive during link measurement. (a) Link measurement setup where the antenna (RX) is integrated in an MDF desk surface, (b) covered by an HPL superstrate and (c) distorted by a laptop or (d) a flash drive. The link measurement is performed by mounting an aligned identical stand-alone version of the antenna (TX) 25 cm above the desktop. The transmit power is set to 0 dBm.

TABLE I
COMPARISON TO STATE OF THE ART ON IMPEDANCE TUNERS.

Item	Frequency (FBW)	Insertion loss [dB]	Tuning technology	Antenna
[11]	400 MHz (>85%)	<0.3	MEMS varactor	None
[12]	586 MHz (<10%)	<1.5	CMOS SC	None
[7]	1/1.25 GHz (>20%)	<1.5	PIN diode switch	None
[9]	2.5 GHz (>20%)	<1.75	PIN diode switch	None
[14]	2.4 GHz (9%)	<1.5	Varactor diode	None
[15]	2.3 GHz (17%)	<4.1	Varactor diode	Stand-alone
[16]	2.45/5.8 GHz (33/9%)	<5.2/0.95	Varactor diode	Modular
[13]	845 MHz (7%)	<1	CMOS SC	Integrated
[8]	1.65 GHz (2%)	<1.5	PIN diode switch	Integrated
This work	**5.5 GHz (46%) (26%)**	**<1.83**	**Varactor diode**	**Stand-alone Integrated**

IV. CONCLUSION

This paper presented a novel AFSIW cavity-backed slot antenna featuring an integrated reconfigurable matching network and implementing the corresponding biasing electronics inside the air-filled cavity without compromising the antenna performance. The output of the integrated matching network achieves 85% of the impedances in the VSWR $\leq$ 3 circle on the Smith chart at the center frequency. The insertion loss remains below 1.83 dB over the entire band of interest, thereby competing with other state of the art impedance tuners. The proposed impedance-tunable antenna features a wide impedance bandwidth from 4.64 GHz to 6.09 GHz. A maximum gain of 4.51 dBi and total antenna efficiency of 57% are achieved at 5.5 GHz. Measurements show that the integration of the biasing circuit in the antenna cavity has almost no influence on the radiation efficiency at the center frequency, thereby proving the potential of cavity-integrated circuitry. The proposed system is compared to a stand-alone antenna in a smart surface desktop scenario while being detuned by objects in its reactive near field, herein achieving a better link budget in four of the six investigated scenarios in the IEEE 802.11ac bands, while significantly improving the return loss at all times.

REFERENCES

[1] T. Qiu, N. Chen, K. Li, M. Atiquzzaman, and W. Zhao, "How Can Heterogeneous Internet of Things Build Our Future: A Survey," *IEEE Communications Surv. & Tut.*, vol. 20, no. 3, pp. 2011–2027, 2018. doi: 10.1109/COMST.2018.2803740

[2] S. Lemey *et al.*, "Threefold Rotationally Symmetric SIW Antenna Array for Ultra-Short-Range MIMO Communication," *IEEE Trans. Antennas Propag.*, vol. 64, no. 5, pp. 1689–1699, 2016. doi: 10.1109/TAP.2016.2536163

[3] N. Claus, J. Verhaevert, and H. Rogier, "High-Performance Air-Filled Multiband Antenna for Seamless Integration Into Smart Surfaces," *IEEE Antennas Wireless Propag. Lett.*, vol. 20, no. 12, pp. 2260–2264, 2021. doi: 10.1109/LAWP.2021.3105908

[4] P. Salonen, Y. Rahmat-Samii, and M. Kivikoski, "Wearable Antennas in the Vicinity of Human Body," in *IEEE Antennas and Propag. Soc. Symp.*, Monterey, CA, USA, 2004, pp. 467–470. doi: 10.1109/APS.2004.1329675

[5] S.-Y. Huang, Y.-S. Cheng, K.-Y. Yang, and R.-B. Wu, "Fast Prediction and Optimal Design for Eye-Height Performance of Mismatched Transmission Lines," *IEEE Trans. Compon. Packag. Manuf. Technol.*, vol. 4, no. 5, pp. 896–904, 2014. doi: 10.1109/TCPMT.2014.2300072

[6] C. Sanchez-Perez, J. de Mingo, P. Garcia-Ducar, P. L. Carro, and A. Valdovinos, "Dynamic load modulation with a reconfigurable matching network for efficiency improvement under antenna mismatch," *IEEE Trans. Circuits Syst. II*, vol. 58, no. 12, pp. 892–896, 2011. doi: 10.1109/TCSII.2011.2172524

[7] T. Zhang, W. Che, and H. Chen, "A Wideband Reconfigurable Impedance Matching Network for Complex Loads," *IEEE Trans. Compon. Packag. Manuf. Technol.*, vol. 8, no. 6, pp. 1073–1081, 2018. doi: 10.1109/TCPMT.2017.2786549

[8] A. Pourghorban Saghati and K. Entesari, "A Reconfigurable SIW Cavity-Backed Slot Antenna With One Octave Tuning Range," *IEEE Trans. Antennas Propag.*, vol. 61, no. 8, pp. 3937–3945, 2013. doi: 10.1109/TAP.2013.2263215

[9] J.-X. Xu, Y.-M. Xue, L. Gao, and X. Y. Zhang, "Switchable filtering circuit with single- and multi-channel operations," *IEEE Trans. Circuits Syst. II*, vol. 67, no. 12, pp. 2958–2962, 2020. doi: 10.1109/TCSII.2020.2993234

[10] R. G. Pesel, S. S. Attar, and R. R. Mansour, "MEMS-Based Switched Capacitor Banks for Impedance Matching Networks," in *Eur. Microw. Conf.*, Paris, France, 2015, pp. 1018–1021. doi: 10.1109/EuMC.2015.7345939

[11] Q. Gu and A. S. Morris, "A New Method for Matching Network Adaptive Control," *IEEE Trans. Microw. Theory Techn.*, vol. 61, no. 1, pp. 587–595, 2013. doi: 10.1109/TMTT.2012.2230022

[12] P. Sjoblom and H. Sjoland, "Measured CMOS Switched High-Quality Capacitors in a Reconfigurable Matching Network," *IEEE Trans. Circuits Syst. II*, vol. 54, no. 10, pp. 858–862, 2007. doi: 10.1109/TCSII.2007.901629

[13] I. Vasilev, J. Lindstrand, V. Plicanic, H. Sjöland, and B. K. Lau, "Experimental Investigation of Adaptive Impedance Matching for a MIMO Terminal With CMOS-SOI Tuners," *IEEE Trans. Microw. Theory Techn.*, vol. 64, no. 5, pp. 1622–1633, 2016. doi: 10.1109/TMTT.2016.2546244

[14] J. A. Estrada, S. Johannes, D. Psychogiou, and Z. Popovic, "Tunable Impedance-Matching Filters," *IEEE Microw. Wireless Compon. Lett.*, vol. 31, no. 8, pp. 993–996, 2021. doi: 10.1109/LMWC.2021.3083184

[15] B. Hur, W. R. Eisenstadt, and K. L. Melde, "Testing and Validation of Adaptive Impedance Matching System for Broadband Antenna," *Electron.*, vol. 8, no. 9, 2019. doi: 10.3390/electronics8091055

[16] S. J. Chen, D. C. Ranasinghe, and C. Fumeaux, "A Robust Snap-On Button Solution for Reconfigurable Wearable Textile Antennas," *IEEE Trans. Antennas Propag.*, vol. 66, no. 9, pp. 4541–4551, 2018. doi: 10.1109/TAP.2018.2851288

[17] K. Y. Kapusuz, S. Lemey, and H. Rogier, "Multipolarization Reconfigurable Air-Filled Substrate Integrated Waveguide Cavity-Backed Slot Antenna," *IEEE Antennas Wireless Propag. Lett.*, vol. 20, no. 4, pp. 622–626, 2021. doi: 10.1109/LAWP.2021.3059449

[18] J.-S. Hong, *Microstrip Filters for RF/Microwave Applications*. Hoboken, NJ, USA: Wiley, 2011, ch. 5, pp. 123–160.

[19] M. Alibakhshikenari *et al.*, "Optimum Power Transfer in RF Front End Systems Using Adaptive Impedance Matching Technique," *Scientific Rep.*, vol. 11, no. 1, p. 11825, 2021. doi: 10.1038/s41598-021-91355-4

[20] A. Petrocchi *et al.*, "An Ultra-Wideband Sensing Board for Radio Frequency Front-End in IoT Transmitters," *Electron.*, vol. 8, no. 10, 2019. doi: 10.3390/electronics8101191